RSC Advances




ROYAL SOCIETY OF CHEMISTRY

www.rsc.org/advances

Journal Name

RSCPublishing

ARTICLE

# Quantitative structure-activity relationships and design of thymine-like inhibitors of thymidine monophosphate kinase of *Mycobacterium tuberculosis* with favorable pharmacokinetic profile

Cite this: DOI: 10.1039/x0xx00000x

Received 00th January 2012,
Accepted 00th January 2012

DOI: 10.1039/x0xx00000x

www.rsc.org/

Keita M. [a,d], Kumar A. [a,b,c], Dali B. [a,d], Megnassan E. [a,d,*], Siddiqi M.I. [a,b], Frecer V. [a,e,f] and Miertus S. [a,f,g]

We have designed new potent inhibitors of thymidine monophosphate kinase of *Mycobacterium tuberculosis* ($TMPK_{mt}$) using structure-based molecular design. Three-dimensional (3D) models of $TMPK_{mt}$-inhibitor complexes were prepared by *in situ* modification of the crystal structure of $TMPK_{mt}$ co-crystallized with the natural substrate deoxythymidine monophosphate (dTMP) (PDB entry code: 1G3U) and a training set of 20 thymine derivatives bearing an aliphatic or aromatic group attached through a spacer (THMDs) with known inhibitory potencies. A QSAR model was elaborated for the training set THMDs and a linear correlation was established between the computed free energies of THMDs binding and observed enzyme inhibition constants ($K_i^{exp}$). Validation of this QSAR model was performed with a 3D-QSAR pharmacophore generation (PH4). Structural information derived from the 3D model and breakdown of computed $TMPK_{mt}$-THMDs interaction energies up to individual active site residue contributions helped us to design new more potent $TMPK_{mt}$ inhibitors. We obtained a reasonable agreement between the free energies of $TMPK_{mt}$-THMDs complexation ($\Delta\Delta G_{com}$) and $K_i^{exp}$ values, which explained approximately 93% of the $TMPK_{mt}$ inhibition data ($pK_i = -0.1422 \cdot \Delta\Delta G_{com} + 4.9199$, $R^2 = 0.93$). Similar agreement was established for the PH4 pharmacophore model ($pK_i^{exp} = 1.0016 \times pK_i^{pre} + 0.0077$, $R^2 = 0.95$). Comparative analysis of the active site residues contributions directed substitutions to various positions of the naphtholactam or naphthosultam moeties and suggested their replacement with phthalimido or isoindolinone or indanone rings, which led to a predicted increase of the inhibitory potency. The predicted $K_i^{pre}$ for the best inhibitor candidate reached the picomolar range for aliphatic acyclic nucleoside analogs and for benzyl pyrimidine-like analogs. This computational approach, which combines molecular modelling, pharmacophore generation and analysis of $TMPK_{mt}$-THMDs interaction energies resulted in a set of proposed $TMPK_{mt}$ inhibitors. It can thus direct medicinal chemists in their search for new antituberculotic agents.

## 1. Introduction

At this moment, we can be quite sure that the millennium development goal to halve the tuberculosis (TB) mortality relative to the 1990 level by 2015 [1], will not be met. On the contrary, the number of countries reporting incidence of cases of multidrug-resistant (MDR) and extensively drug-resistant (XDR) tuberculosis, which are resistant to almost all fluoroquinolones plus the injectable antituberculotics, kanamycin, amikacin or capreomycin, is growing [2]. Therefore, it becomes crucial to analyse why the TB burden increases despite treatment and past and current vaccination efforts.

According to WHO, Sub-Saharan Africa has the highest rates of TB driven primarily by the HIV co-infection, while approximately 2 billion individuals worldwide suffer from a latent mycobacterium infection and are at risk of developing active tuberculosis [3].

Thymidine monophosphate kinase ($TMPK_{mt}$) was recognized as a validated pharmacological target ($TMPK_{mt}$ is an essential enzyme for the synthesis of thymidine diphosphate from deoxythymidine monophosphate (dTMP) that is needed for DNA synthesis and replication). $TMPK_{mt}$ inhibitors block the replication of the mycobacterium [4]. So far, the most potent thymidine-derived inhibitors (THMD) reported in the literature exert their inhibitory activity in the low micromolar range

(3.5 – 5μM) [5]. More potent reported THMDs with inhibition constants within 0.27 - 0.75 μM contain aliphatic spacer linking the thymine base to the distal naphtholactam or naphthosultam moieties [6]. Similarly, THMDs with aromatic spacers reached an inhibitory concentration range of 6.5 - 10 μM. Some THMD structures are shown in Figure 1.

The availability of X-rays crystal structures of the TMPK$_{mt}$ enzyme bound to its substrate as well as to several THMDs opened the gate to structure-based design of new antituberculotic agents sharing similar mode of action [7].

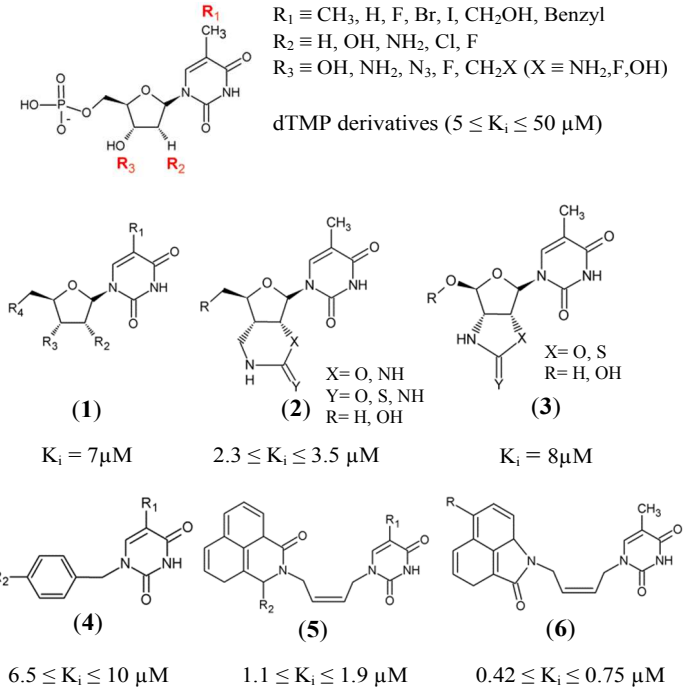


**Figure 1:** Structures of known TMPK$_{mt}$ inhibitors.

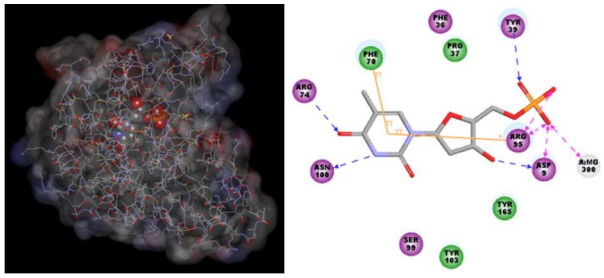

**Figure 2:** Interaction map of dTMP with active site residues (right) and location of the active site (CPK representation of dTMP) in the 3D model of TMPK$_{mt}$ (left).

Structure-based design of TMPK$_{mt}$ inhibitors can start with assessment of enzyme-ligand interaction maps (Figure 2), which can be extracted from high resolution crystal structures of TMPK$_{mt}$ - dTMP complexes, such as 1GSI [8] and 1G3U [9] [10, 11]. The maps show the pyrimidine ring of the thymine in a π - π stacking interaction with Phe70 and a hydrogen bond with Arg74 keeping the orientation of the pyrimidine ring, while the hydroxyl group of the ribose ring is hydrogen bonded to Asp9. The phosphate group is kept in its position by electrostatic interactions with the $Mg^{2+}$ ion and by hydrogen bonding to Arg95. On the basis of this structural information dTMP analogs were proposed with the phosphate group replaced by anionic isosteres and bearing bromine substitution on the pyrimidine ring intended to improve the ADME profile of the compounds [5, 12] (Figure 1, molecules (**1**) to (**6**)). The dTMP analogs with alkene linkers replacing the ribose moiety and dibenzoindolone or dibenzoquinolone rings exploring the edge to face interaction between the naphtyl group and the selective Tyr39 residue (**5**) and (**6**) represent submicromolar inhibitors of the TMPK$_{mt}$ [6]. In a recent computational inhibitor design study a dTMP analogue with a carboxylate group in the 5'-position of the ribose ring was predicted to shift the inhibitory potency up to the nanomolar concentration range ($K_i^{pre}$ = 0.155 nM; Fig. 3, inhibitor A) [11].

In this work we have extended the structure-based design of TMPK$_{mt}$ inhibitors and propose analogs that contain aromatic moieties attached by aliphatic or aromatic spacers to the thymine, which interact with the side chains of residues Tyr103, Tyr165 and Tyr39. A Hansch-type QSAR model of inhibitor-enzyme interaction was built for a training set of 20 known THMDs, which correlates computed Gibbs free energy of the enzyme-inhibitor complex formation with the experimental inhibition constants [6, 12, 13]. In addition a 3D-QSAR model was used to prepare a four-feature pharmacophore (PH4) of the THMDs. The predictive power of the QSAR model of inhibitor-enzyme binding was cross-checked with the PH4 3D-QSAR pharmacophore model. This was used to screen a set of modelled thymidine analogs for potent TMPK$_{mt}$ inhibitors. The virtual hits identified by the complexation QSAR model reached predicted activities within subnanomolar concentration range.

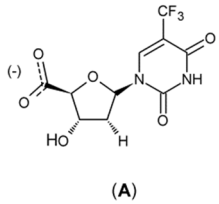


**Figure 3:** Chemical structure of proposed nanomolar inhibitor A [11].

# 2. Methods

### 2.1 Training and validation sets

The training and validation sets of thymine-like inhibitors of TMPK$_{mt}$ used in this study were taken from the literature [6, 12, 13]. The inhibitory potencies of these derivatives cover sufficiently broad range of activity to allow a reliable QSAR model to be built (0.27 μM ≤ $K_i^{exp}$ ≤ 202 μM).

### 2.2 Model building

Molecular models of the enzyme-inhibitor complexes (E:I), free TMPK$_{mt}$ (E) and inhibitors (I) were prepared from the high-resolution crystal structure (1.95Å) of a reference complex containing the deoxythymidine monophosphate (dTMP) bound to TMPK$_{mt}$ [8] (Protein Data Bank [14] entry code 1G3U) using Discovery Studio 2.5 molecular modelling program [15]. The structures of E and E:I complexes were considered to be at the pH of 7 with neutral N- and C-terminal residues and all protonizable and ionizable residues charged. No crystallographic water molecules were included into the model. The inhibitors were built into the reference structure by *in situ* replacing of the derivatized groups of the dTMP moiety (molecular scaffold). An exhaustive conformational search over all rotatable bonds of the replacing function group coupled with a careful gradual energy-minimization of the modified inhibitor and active site residues of the TMPK$_{mt}$ located in the vicinity of

the inhibitor (within 5 Å distance), was employed to identify low-energy bound conformations of the modified inhibitor. The resulting low-energy structures of the E:I complexes were then carefully refined by minimization of the whole complex. This procedure has been successfully used for model building of viral, bacterial and protozoal enzyme-inhibitor complexes and design of peptidomimetic, hydroxynaphthoic and thymidine inhibitors [11, 16, 17, 18, 19, 20].

### 2.3 Molecular mechanics

Modelling of inhibitors, TMPK$_{mt}$ and complexes was carried out in all-atom representation using atomic and charge parameters of the CHARMm force field [15]. A dielectric constant of 4 was used for all molecular mechanics (MM) calculations in order to take into account the dielectric shielding effect in proteins. Minimizations of the E:I complexes, free E and I were carried out by relaxing the structures gradually, starting with the added hydrogen atoms, continued with inhibitor heavy atoms, followed by residue side chains and concluded with protein backbone relaxation. In all the geometry optimizations, a sufficient number of steepest descent and conjugate gradient iterative cycles were used with the convergence criterion for the average gradient set to 0.01 kcal.mol$^{-1}$.Å$^{-1}$.

### 2.4 Conformational search

Free inhibitor conformations were derived from their bound conformations in the E:I complexes by gradual relaxation to the nearest local energy minimum. Then a Monte Carlo search (with an upper limit of 50 000 iterations) for low-energy conformations over all rotatable bonds except those in the rings was carried out using Discovery Studio [15]. Two hundred unique conformations were generated for each inhibitor by randomly varying torsion angles of the last accepted conformer by ±15° at 5000 K followed by subsequent energy minimization. During the minimization a dielectric constant $\varepsilon$ = 80 was used to account approximately for the dielectric screening effect of hydration upon the generated conformers. The conformer with the lowest total energy was selected and re-minimized at $\varepsilon$ = 4.

### 2.5 Solvation Gibbs free energies

The electrostatic component of solvation Gibbs free energy that includes also the effects of ionic strength via solving nonlinear Poisson-Boltzmann equation [21,22] was computed by the DelPhi module in Discovery Studio [15]. The program treats the solvent as a continuous medium of high dielectric constant ($\varepsilon_o$ = 80) and the solute as a cavity of low dielectric ($\varepsilon_i$ = 4) with boundaries linked to the solute's molecular surface, which encloses the solute's atomic charges. The program uses a finite difference method to numerically solve for the molecular electrostatic potential and reaction field around the solute. DelPhi calculations were carried out on a (235 × 235 × 235) cubic lattice grid for the E:I complexes and free E and (65 × 65 × 65) grid for the free I with full coulombic boundary conditions. Two subsequent focusing steps led in both cases to a similar final resolution of about 0.3 Å per grid unit at 70% filling of the grid by the solute. Physiological ionic strength of 0.145 mol.dm$^{-3}$, atomic partial charges and radii defined in the CHARMm parameter set [15] and a probe sphere radius of 1.4 Å were used. The electrostatic component of the solvation Gibbs free energy was calculated as the reaction field energy [21, 23, 24, 25].

### 2.6 Calculation of binding affinity

Inhibition constant ($K_i$) of a reversible inhibitor I is related to the standard Gibbs free energy (GFE) change of the formation of E:I complex ($\Delta G_{com}$) in a solvent. The $K_i$ value can thus be predicted from the complexation GFE as $\Delta G_{com} = -RT\ln K_i$ assuming the following equilibrium:

$$\{E\}_{aq} + \{I\}_{aq} \leftrightarrow \{E:I\}_{aq} \quad (1)$$

where $\{\}_{aq}$ indicates solvated species. The standard GFE change of reaction (1) can be derived by molecular simulations of the complex and the free reactants:

$$\Delta G_{com} = G\{E:I\} - G\{E\} - G\{I\} \quad (2)$$

In this work we approximate the exact values of standard GFE for larger systems such as enzyme-inhibitor complexes by the expression [18-19]:

$$G\{E:I\} \approx E_{MM}\{E:I\} + RT - TS_{trv}\{E:I\} + G_{sol}\{E:I\} \quad (3)$$

where $E_{MM}\{E:I\}$ stands for the molecular mechanics total energy of the complex (including bonding and non-bonding contributions), $G_{sol}\{E:I\}$ is the solvation GFE and $TS_{trv}\{E:I\}$ is the entropic term:

$$TS_{trv}\{E:I\} = TS_{tran}\{E:I\} + TS_{rot}\{E:I\} + TS_{vib}\{E:I\} \quad (4)$$

composed of a sum of contributions arising from translational, rotational and vibrational motions of E:I. Assuming that the *tran* and *rot* terms for the complex E:I and free enzyme E are approximately equal, we obtain:

$$\Delta G_{com} \approx [E_{MM}\{E:I\}-E_{MM}\{E\}-E_{MM}\{I\}] + [G_{sol}\{E:I\}-G_{sol}\{E\}-G_{sol}\{I\}] + TS_{tran}\{I\} + TS_{rot}\{I\} - [TS_{vib}\{E:I\}-TS_{vib}\{E\}-TS_{vib}\{I\}] = \Delta H_{MM} + TS_{tran}\{I\} + TS_{rot}\{I\} - \Delta TS_{vib} + \Delta G_{sol} \quad (5)$$

where $TS_{tran}\{I\}$ and $TS_{rot}\{I\}$ describe the translational and rotational entropy terms of the free inhibitor and $\Delta TS_{vib}$ represents a simplified vibrational entropy change upon the complex formation: $\Delta TS_{vib} = TS_{vib}\{I\}_E - TS_{vib}\{I\}$ [26, 27]. Comparison between different inhibitors was done via relative changes in the complexation GFE with respect to a reference inhibitor, $I_{ref}$, assuming ideal gas behaviour for the rotational and translational motions of the inhibitors:

$$\Delta\Delta G_{com} = \Delta G_{com}(I) - \Delta G_{com}(I_{ref}) = \Delta\Delta H_{MM} - \Delta\Delta TS_{vib} + \Delta\Delta G_{sol} \quad (6)$$

The binding energy calculation protocol in Discovery Studio 2.5.5 (the latest version of DS 2.5) can now compute the loss of conformational entropy of a bound ligand [28]. This term is denoted $\Delta\Delta$TS in tables 2 and 5. The use of the entropic contribution leads to a more accurate evaluation of the relative binding affinity.

The evaluation of relative changes is preferable as it is expected to lead to partial cancellation of errors caused by the approximate nature of the molecular mechanics method as well as solvent and entropic effects description.

### 2.7 Interaction energy

To calculate the MM interaction energy ($E_{int}$) between enzyme residues and the inhibitor, a protocol available in Discovery Studio 2.5 [15] that computes the non-bonded interactions (van der Waals and electrostatic terms) between defined sets of atoms, was used. The calculations were performed using CHARMm force field [15] with a dielectric constant of 4. The breakdown of $E_{int}$ into active site residue contributions (presented in % of total $E_{int}$ of TMPK*mt*-THMD) reveals the significance of individual interactions and allows a comparative analysis, which leads to identification of affinity enhancing and unfavourable THMD substitutions.

### 2.8 Pharmacophore generation

Pharmacophore modelling assumes that a set of structural features in a molecule is recognized by the receptor and is responsible for the molecule's biological activity. Bound conformations of inhibitors taken from the models of E:I complexes were used for building of 3D-QSAR pharmacophore by means of Catalyst HypoGen algorithm [29] implemented in Discovery Studio 2.5 [15]. The top scoring pharmacophore hypothesis was built up in three stages (constructive, subtractive and optimization step) from the set of the most active inhibitors. Inactive molecules served for definition of the excluded volume. The maximum number of five features allowed by the HypoGen algorithm was selected based on the THMD scaffold and substituents during the pharmacophore generation, namely: hydrophobic aromatic (HYdAr), hydrophobic aliphatic (HYd), hydrogen-bond donor, (HBD), hydrogen-bond acceptor (HBA) and ring aromatic (Ar). Adjustable parameters of the protocol were kept at their default values except the uncertainty on the activity, which was set to 1.25 instead of 3. This parameter choice was intended to bring the uncertainty interval of experimental activity from wide span $\langle K_i/3, 3\times K_i\rangle$ to a relatively narrow one $\langle 4\times K_i/5, 5\times K_i/4\rangle$ taking thus into account the accuracy and homogeneity of the measured inhibitory activities which are coming from the same laboratory. During generation of 10 pharmacophores the number of missing features was set to 0. The best pharmacophore model was selected.

### 2.9 ADME-related Properties

Pharmacokinetics properties such as octanol/water partitioning coefficient, aqueous solubility, blood/brain partition coefficient, Caco-2 cell permeability, serum protein binding, number of likely metabolic reactions, and another eighteen descriptors related to adsorption, distribution, metabolism and excretion (ADME properties) of the inhibitors were computed by the QikProp program [30] based on the method of Jorgensen [31,32,33]. In this approach, experimental results of more than 710 compounds including about 500 drugs and related heterocycles were used to produce regression equations correlating experimental and computed descriptors resulting in an accurate prediction of molecule's pharmacokinetic properties. Drug likeness (#stars) - the number of property descriptors that fall outside the range of values determined for 95 % of known drugs out of 24 selected descriptors computed by the QikProp [30], was used as an additional ADME-related compound selection criterion – the druglikeness.

**Table 1.** Training and validation sets of THMDs for the QSAR model

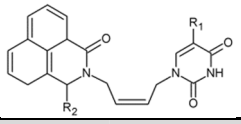

| Inhibitor | $R_1$ | $R_2$ | $K_i$ (μM) |
|---|---|---|---|
| THMD1 | $CH_3$ | =O | 1.9 |
| THMD2 | $CH_3$ | -OH | 4.7 |
| THMD3 | $CH_3$ | $-OCH_3$ | 6.2 |
| THMD4 | H | =O | 1.4 |
| THMD5 | H | $NO_2$ | 0.42 |
| THMD6 | $NO_2$ | $SO_2$ | 0.75 |
| THMD7 | $SO_2$ | | 0.27 |

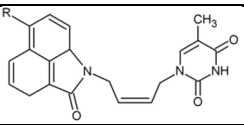

| Inhibitor | R | $K_i$ (μM) |
|---|---|---|
| THMV1 | $NCHCOCH_3$ | 6 |
| THMV3 | $NH_2$ | 2.4 |

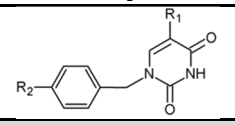

| Inhibitor | $R_1$ | $R_2$ | $K_i$ (μM) |
|---|---|---|---|
| THMD8 | $CH_3$ | $CH_2CH_2CONH_2$ | 89 |
| THMD9 | $CH_3$ | $CH_2CH_2COOH$ | 55 |
| THMD10 | $CH_3$ | $CH{=}CHCONH_2$ | 195 |
| THMD11 | $CH_3$ | $(CH_2)_3CONH_2$ | 112 |
| THMD12 | $CH_3$ | $C{\equiv}CCH_2CH_2OH$ | 70 |
| THMD13 | Br | $(CH_2)_3COOH$ | 10 |
| THMD14 | $CH_3$ | Br | 38 |
| THMD15 | H | $(CH_2)_3COOH$ | 202 |
| THMD16 | Cl | $(CH_2)_3COOH$ | 6.5 |
| THMD17 | $CH_3$ | $(CH_2)_3COOH$ | 13 |
| THMD18 | Cl | $(CH_2)_3CONH_2$ | 39 |
| THMD19 | Cl | $(CH_2)_4COOH$ | 16 |
| THMD20 | Br | $(CH_2)_4CONH_2$ | 35 |

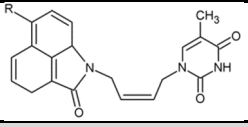

| Inhibitor | $R_1$ | $R_2$ | $K_i$ (μM) |
|---|---|---|---|
| THMV2 | Br | $(CH_2)_3CONH_2$ | 39 |

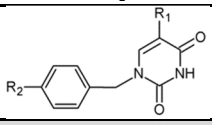

## 3. Results and discussion

A training set of 20 THMDs (Table 1) and validation set of 3 THMVs (Table 1) were selected from 3 series of $TMPK_{mt}$ inhibitors with experimentally determined activities studied in the same laboratory [6, 12, 13]. Their experimental inhibition constants $K_i^{exp}$ cover a concentration range sufficiently large (0.27 – 202 μM) to serve well for building of a useful QSAR model of $TMPK_{mt}$ inhibition.

### *QSAR model*

The relative Gibbs free energy of the E:I complex formation, equation (6), was computed for the complexes prepared by *in situ* modification of the template inhibitor dTMP in the binding site of $TMPK_{mt}$ as described in the Methods section. Table 2 lists the $\Delta\Delta G_{com}$ of E:I binding and its components, equation (6). Since it is computed in an approximate way, the relevance of the binding model is evaluated through a correlation with the experimental activity data ($K_i^{exp}$) by a linear regression. The statistical data of the obtained regression equation are presented in Figure 3A and listed in Table 3. Relatively high values of the regression coefficient and Fischer F-test indicate that there is a strong relationship between the binding model and the observed inhibitory potencies of the THMDs. The ratio of predicted and observed inhibition constants ($K_i^{pre}/K_i^{exp}$) for the validation set of THMVs (not included into the training set) is close to one and documents considerable predictive power of the QSAR model. Therefore, the regression equation and computed $\Delta\Delta G_{com}$ quantities can be used to predict $TMPK_{mt}$ inhibition constants

$K_i^{pre}$ of novel THMD analogs, provided that the analogs share the same binding mode with the training set compounds.

To identify chemical modifications of THMDs leading to new inhibitor structures with high predicted binding to TMPK*mt*, we have analyzed contributions of individual residues of the enzyme binding pocket to the total computed enzyme-inhibitor interaction energy ($E_{int}$). In this way we have noticed a significant contribution to the $E_{int}$ from residues Phe70, Arg95, Ser99 with a strong variation of the contributions of Arg153 and Arg160 for the highly active THMDs (Figure 6) and less active inhibitors (Figure 7).

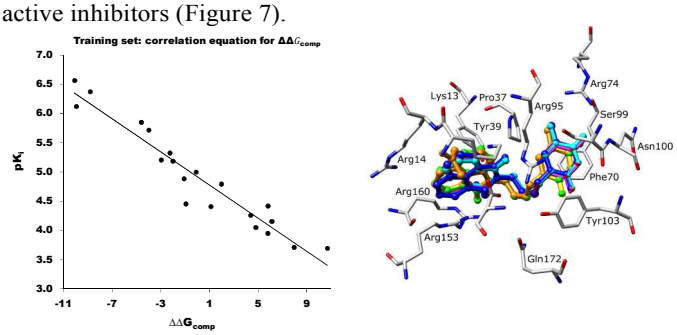


A B

**Figure 3**. **A.** Plot of the correlation equation between $pK_i$ and relative complexation Gibbs free energies $\Delta\Delta G_{com}$ [kcal/mol] of the training set. **B.** Superimposition of optimized bound conformations of highly active training set compounds.

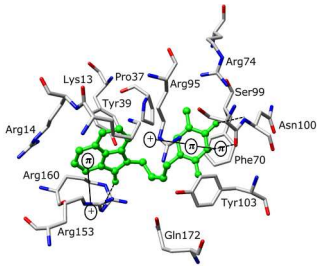


**Figure 4.** Close-up of one of the most active training set inhibitor THMD5 (green color) at the active site of TMPK*mt*. Hydrogen bonds are shown in dashed black lines, other interactions are displayed as solid black lines.

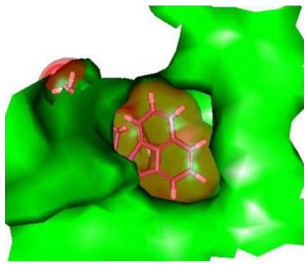

**Figure 5.** Naphtholactam moiety in stick representation fitted into the binding pocket of the TMPK*mt*. Solid molecular surface of the active site is shown in green colour.

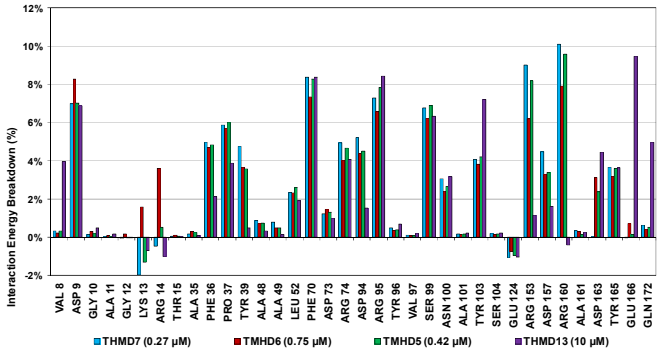


**Figure 6.** Interaction energy breakdown (in % of the total $E_{int}$ of TMPK*mt*:THMD) to residue contributions for highly active training set THMDs.

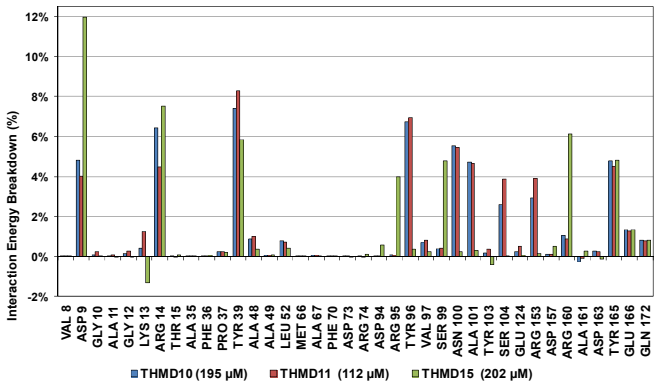


**Figure 7.** Interaction energy breakdown (in % of the total $E_{int}$ of TMPK*mt*:THMD) to residue contributions for less active training set THMDs.

## *Binding mode of inhibitors*

The binding mode of THMDs in the active site of TMPK*mt* present in the crystal structures of TMPK*mt*-dTMP complexes [7, 8, 9] which was used in the complexation model of inhibitors THMD1-THMD20 is illustrated in Figures 4 and 5. In this model the main electrostatic and hydrogen bonding interactions of the phosphate moiety of dTMP with residues Arg95 (and Tyr39) are preserved (Figure 6). The stacking interaction of the pyrimidine ring with Phe70 is kept along with the cation-aromatic π interaction with Arg95 and Arg153. This last interaction is probably the main driving force of the increase of affinity of the submicromolar inhibitors THMD5-THMD7 with the TMPK*mt*. A comparison of the interaction patterns of Figures 6 and 7 highlights the main stabilizing contributions of individual residues to the $E_{int}$ (in % of the total $E_{int}$ of TMPK*mt*:THMD) for the highly active THMDs (*h*THMDs) namely THMD5 (0.42 μM), THMD6 (0.75 μM), THMD7 (0.27 μM) and THMD13 (10 μM) (Figure 6) and for less active ones (*l*THMDs) THMD10 (195 μM), THMD11 (112 μM) and THMD15 (202 μM) (Figure 7). The essential contributions of residues to $E_{int}$ expressed in % of total $E_{int}$ for *h*THMDs vs. *l*THMDs for Phe36 (5% vs. 0%), Pro37 (6% vs. 0%), Phe70 (8% vs. 0%), Arg74 (5% vs. 0%), Asp94 (5% vs. 1%), Arg95 (8% vs. 4%), Arg153 (8% vs. 3%) and Arg160 (10% vs. 4%) known to be significant to the binding of the potent analogs globally are missing for the less active THMDs. Oppositely Tyr96 (0% vs. 7%) contribution is missing for *h*THMDs can be used for the design of new potent analogs. A refined analysis of *h*THMDs (Figure 6) reveals the essential contribution specific to aromatic spacer THMDs (*ar*THMDs) and missing for aliphatic spacer THMDs (*al*THMDs): Glu166 (9% for THMD13 vs. 0% for THMD5-7), Gln172 (5% vs. 1%) and Val8 (4% vs. 0%). Improvement in the contribution of these last three residues lead to more potent *ar*THMDs analogs exemplified by THMA49 and 50. The increased contribution of Tyr103 (7% for THMD13 vs. 4% for THMD5-7) is due to additional aromatic π - π interaction with the aromatic spacer as depicted in 2D in Figure 10.

For *al*THMDs Figures 4 and 6 indicate that positions 6 and 7 of the naphtholactam are suitable for favourable interactions with Lys13 while positions 4 and 5 can be used for interaction with Arg14.

**Table 2.** Complexation Gibbs free energy (binding affinity) and its components for the training set of TMPK$_{mt}$ inhibitors THMD1-20 and validation set inhibitors THMV1-3.

| Training Set[a] | $M_w$[b] [g/mol] | $\Delta\Delta H_{MM}$[c] [kcal/mol] | $\Delta\Delta G_{sol}$[d] [kcal/mol] | $\Delta\Delta TS$[e] [kcal/mol] | $\Delta\Delta G_{com}$[f] [kcal/mol] | $K_i^{exp}$[g] [μM] |
|---|---|---|---|---|---|---|
| THMD1 | 375 | -1.40 | -1.67 | 0.93 | -4 | 1.9 |
| THMD2 | 439 | -4.32 | 3.02 | 0.96 | -2.26 | 4.7 |
| THMD3 | 377 | -6.36 | 4.42 | 1.04 | -2.98 | 6.2 |
| THMD4 | 391 | -4.25 | 0.49 | 0.85 | -4.61 | 1.4 |
| THMD5 | 361 | -18.42 | 10.36 | 0.75 | -8.81 | 0.42 |
| THMD6 | 392 | -24.14 | 15.30 | 1.11 | -9.95 | 0.75 |
| THMD7 | 383 | -20.63 | 11.47 | 0.94 | -10.09 | 0.27 |
| THMD8 | 287 | 1.69 | 3.47 | 0.36 | 4.8 | 89 |
| THMD9 | 288 | 1.46 | 3.29 | 0.37 | 4.38 | 55 |
| THMD10 | 285 | 2.96 | 5.35 | 0.37 | 7.94 | 195 |
| THMD11 | 301 | 1.36 | 4.97 | 0.54 | 5.79 | 112 |
| THMD12 | 284 | 3.33 | 3.22 | 0.43 | 6.12 | 70 |
| THMD13 | 366 | -18.90 | 19.80 | 1 | -0.1 | 10 |
| THMD14 | 294 | 6.36 | 0.55 | 1.11 | 5.8 | 38 |
| THMD15 | 288 | 3.04 | 8.09 | 0.44 | 10.69 | 202 |
| THMD16 | 323 | -16.93 | 15.66 | 0.73 | -2.01 | 6.5 |
| THMD17 | 302 | -9.20 | 8.65 | 0.55 | -1.1 | 13 |
| THMD18 | 322 | -7.83 | 9.66 | 0.73 | 1.1 | 39 |
| THMD19 | 337 | -5.59 | 8.44 | 0.88 | 1.97 | 16 |
| THMD20 | 380 | -19.70 | 19.87 | 1.11 | -0.95 | 35 |
| **Validation Set** | **$M_w$** [g/mol] | **$\Delta\Delta H_{MM}$** [kcal/mol] | **$\Delta\Delta G_{sol}$** [kcal/mol] | **$\Delta\Delta TS$** [kcal/mol] | **$\Delta\Delta G_{com}$** [kcal/mol] | **$K_i^{pre}/K_i^{exp}$**[h] |
| THMV1 | 404 | -18.51 | 17.30 | 1.21 | -2.42 | 0.907 |
| THMV2 | 366 | -9.04 | 13.08 | 1.00 | 3.05 | 0.837 |
| THMV3 | 362 | -17.38 | 13.50 | 0.88 | -4.76 | 1.054 |

[a] for the chemical structures of the training and validation sets of inhibitors see Table 1;
[b] $M_w$ is the molecular mass of the inhibitor;
[c] $\Delta\Delta H_{MM}$ is the relative enthalpic contribution to the Gibbs free energy change related to the TMPK$_{mt}$:THMD complex formation derived by molecular mechanics (MM): $\Delta\Delta H_{MM} \cong [E_{MM}\{TMPK_{mt}:THMDx\} - E_{MM}\{THMDx\}] - [E_{MM}\{TMPK_{mt}:THMD0\} - E_{MM}\{THMD0\}]$, THMD0 – is the reference inhibitor molecule (1) with $R_1$=Me, $R_2$=H, $R_3$=OH and $R_4$=$N_3$;
[d] $\Delta\Delta G_{solv}$ is the relative solvation Gibbs free energy contribution to the Gibbs free energy change related to TMPK$_{mt}$:THMD complex formation: $\Delta\Delta G_{sol} = [G_{sol}\{TMPK_{mt}:THMDx\} - G_{sol}\{THMDx\}] - [G_{sol}\{TMPK_{mt}:THMD0\} - G_{sol}\{THMD0\}]$;
[d] $\Delta\Delta TS$ is the relative entropic contribution of the inhibitor to the Gibbs free energy related to protease-inhibitor complex formation: $\Delta\Delta TS = [TS\{TMPK_{mt}:THMDx\} - TS\{THMDx\}] - [TS\{TMPK_{mt}:THMD0\} - TS\{THMD0\}]$;
[f] $\Delta\Delta G_{com}$ is the relative Gibbs free energy change related to the enzyme-inhibitor complex formation: $\Delta\Delta G_{com} \cong \Delta\Delta H_{MM} + \Delta\Delta G_{sol} - \Delta\Delta TS_{vib}$.
[g] $K_i^{exp}$ is the experimental TMPK$_{mt}$ inhibition constant taken from reference [6,12,13].
[h] ratio of predicted and experimental inhibition constants $K_i^{pre}/K_i^{exp}$. $K_i^{pre}$ was derived from $pK_i^{pre} = -\log_{10}(K_i^{pre})$ which was predicted from computed $\Delta\Delta G_{com}$ using the regression equation shown in Table 3.

**Table 3.** Regression analysis of computed binding affinities $\Delta\Delta G_{com}$ and experimental inhibition constants $pK_i^{exp} = -\log_{10}(K_i^{exp})$ of THMDs towards TMPK$_{mt}$.

| Statistical Data of Regression | |
|---|---|
| $pK_i = -0.1422 \cdot \Delta\Delta G_{com} + 4.9199$ | |
| Number of compounds n | 20 |
| Squared correlation coefficient of regression $R^2$ | 0.93 |
| Cross-validated squared correlation coefficient $R^2_{XV}$ | 0.92 |
| Standard error of regression σ | 0.248 |
| Statistical significance of regression, Fischer F-test | 218.9 |
| Level of statistical significance α | > 95% |
| Range of activity of $K_i^{exp}$ [μM] | 0.27 - 202 |

## *Pharmacophore model of inhibitory activity*

The 3D-QSAR PH4 pharmacophore generation process follows three main steps, the constructive, the subtractive and the optimization steps. The constructive phase of HypoGen automatically selected as leads the most active compounds for which $0.27 \times 1.25 - K_i^{exp}/1.25 > 0$, namely $0.27 \le K_i^{exp} \le 0.42$ μM, THMD5 and THMD7 were used to generate all starting PH4 features and only those features were retained which matched both leads THMD5, THMD7. In the subtractive phase the inactive compounds with $\log_{10}(K_i^{exp}) - \log_{10}(0.27) > 3.5$ were used to remove those pharmacophoric features that mapped more than 50% of these compounds, while pharmacophore representatives which contained all five features were retained. In the optimization phase, only the highest scoring PH4s based on their probability function cost which was calculated by a simulated annealing protocol, were retained. A total of 10 optimized hypotheses were kept all displaying four features. The costs ranged from 89.7 (Hypo1) to 190.5 (Hypo10). The relatively small gap between the highest and the lowest cost corresponds well with the homogeneity of the generated hypotheses and the consistency of the training set. For this PH4 the fixed cost (47.9) is lower than the null cost (810.3) by a difference $\Delta = 762.4$. This difference is a major quality indicator of the PH4 predictability (it has to be noted that $\Delta > 70$ corresponds to an excellent chance or a probability higher than 90% that the model represents a true correlation [15]). To be statistically significant the hypotheses have to be as close as possible to the fixed cost and as far as possible from the null cost. For the set of 10 hypotheses the difference was larger or equal to 762.4, which attests high quality of the pharmacophore model. The standard indicators as the root-mean-square deviations (RMSD) between the hypotheses range from 1.998 to 3.732 and the squared correlation coefficient ($R^2$) falls to an interval from 0.97 to 0.91. The first PH4 hypothesis with the best cost, RMSD and $R^2$ was retained for further analysis. The statistical data for the set of hypotheses (costs, RMSD, R) are listed in Table 4. The regression equation for Hypo1: $pK_i^{exp} = 1.0016 \times pK_i^{pre} + 0.0077$ ($n = 20$, $R^2 = 0.95$, $R^2_{XV} = 0.94$, $F = 330.8$, $\sigma = 0.204$, $\alpha > 95\%$) is plotted in Figure 8. The figure shows also the geometry of the Hypo1 PH4 and the THMV3 inhibitor mapping to it. To check the consistency of the generated pharmacophore model we have calculated the ratio of predicted and observed activities ($K_i^{pre}/K_i^{exp}$) for the validation set. The computed ratios were as follows: THMV1, 1.019; THMV2, 0.918; THMV3, 1.068; all of them lie relatively close to one, which documents a substantial predictive power of the regression for the best PH4 model. The randomization validation of the PH4 model was also carried out by the CatScramble algorithm in the Catalyst for 49 random runs corresponding to 98% confidence level. This procedure created 10 valid hypotheses for each run, however, none of them was as predictive as the Hypo10, the hypothesis with the highest cost is shown in Table 4. Thus there is a 98% probability that the best selected hypothesis Hypo1 represents a pharmacophore model for the biological activity of THMDs within the same level of predictive power as the complexation model, which relies on the 3D structures of the TMPK$_{mt}$:THMDx complexes and computed Gibbs free energies of the enzyme-inhibitor binding $\Delta\Delta G_{com}$.

**Table 4.** Output parameters of 10 generated PH4 pharmacophoric hypotheses after CatScramble validation procedure for TMPK$_{mt}$ inhibitors listing RMSD, total cost and correlation coefficient R

| Hypothesis | RMSD | R | Total Cost |
|---|---|---|---|
| Hypo1 | 1.998 | 0.97 | 89.7 |
| Hypo2 | 2.733 | 0.95 | 123.9 |
| Hypo3 | 2.921 | 0.94 | 135.2 |
| Hypo4 | 3.038 | 0.94 | 141.4 |
| Hypo5 | 3.182 | 0.93 | 150.1 |

| | | | |
|---|---|---|---|
| Hypo6 | 3.701 | 0.91 | 188.1 |
| Hypo7 | 3.699 | 0.91 | 188.3 |
| Hypo8 | 3.703 | 0.91 | 188.8 |
| Hypo9 | 3.707 | 0.91 | 188.9 |
| Hypo10 | 3.732 | 0.91 | 190.5 |
| Fixed Cost | 0.0 | 1.0 | 47.9 |
| Null Cost | 8.802 | 0.0 | 810.3 |

**Table 5.** Designed THMD analogs (THMA1-50) and their predicted inhibitory activities ($K_i^{pre}$) against $TMPK_{mt}$

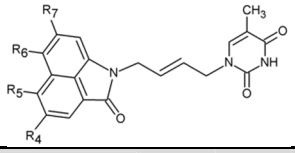


| Inhibitor | Structure | | | | $\Delta\Delta H_{MM}$ | $\Delta\Delta G_{sol}$ | $\Delta\Delta TS$ | $\Delta\Delta G_{com}$ | $K_i^{pre}$ [nM] |
|---|---|---|---|---|---|---|---|---|---|
| | $R_4$ | $R_5$ | $R_6$ | $R_7$ | | | | | |
| THMA1 | H | H | OH | H | -24.72 | 10.19 | 0.90 | -15.43 | 77 |
| THMA2 | H | H | H | OH | -26.14 | 9.37 | 0.87 | -17.64 | 37 |
| THMA3 | H | $CH_2OH$ | H | H | -24.05 | 5.27 | 1.01 | -19.8 | 18 |
| THMA4 | H | H | $CH_2OH$ | H | -24.59 | 6.39 | 1.02 | -19.23 | 22 |
| THMA5 | H | H | H | $CH_2OH$ | -23.89 | 4.91 | 0.96 | -19.93 | 18 |
| THMA6 | H | $CH_2OH$ | $CH_2OH$ | H | -24.52 | 1.51 | 1.21 | -24.22 | 4 |
| THMA7 | H | H | $SO_2Cl$ | H | -32.57 | 11.41 | 1.45 | -22.61 | 7 |
| THMA8 | H | H | Cl | H | -21.50 | 3.57 | 1.05 | -18.97 | 24 |
| THMA9 | H | H | F | H | -21.36 | 3.61 | 0.91 | -18.66 | 27 |
| THMA10 | H | H | Br | H | -21.16 | 3.40 | 1.31 | -19.07 | 23 |
| THMA11 | H | H | Cl | Cl | -19.56 | 3.50 | 0.90 | -15.43 | 77 |

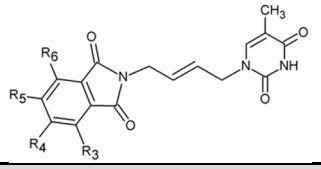


| Inhibitor | Structure | | | | $\Delta\Delta H_{MM}$ | $\Delta\Delta G_{sol}$ | $\Delta\Delta TS$ | $\Delta\Delta G_{com}$ | $K_i^{pre}$ [nM] |
|---|---|---|---|---|---|---|---|---|---|
| | $R_3$ | $R_4$ | $R_5$ | $R_6$ | | | | | |
| THMA12 | H | H | H | H | -29.51 | 12.06 | 0.56 | -18.02 | 33 |
| THMA13 | H | $NHCOCH_3$ | H | H | -27.33 | 11.10 | 1.05 | -17.28 | 42 |
| THMA14 | H | $NO_2$ | H | H | -24.51 | 12.29 | 0.56 | -12.78 | 183 |
| THMA15 | H | $NH_2$ | H | H | -25.82 | 8.09 | 0.71 | -18.44 | 29 |
| THMA16 | H | COO(-) | H | H | -31.87 | 6.95 | 0.99 | -23.14 | 6 |
| THMA16' | H | H | COO(-) | H | -24.17 | 4.40 | 0.99 | -20.76 | 13 |
| THMA17 | H | $OCH_3$ | H | H | -28.90 | 4.92 | 0.85 | -24.82 | 4 |
| THMA18 | $OCH_3$ | $OCH_3$ | H | H | -30.62 | 9.18 | 1.03 | -22.48 | 8 |
| THMA19 | $OCH_3$ | H | $OCH_3$ | H | -29.87 | 12.65 | 1.08 | -18.3 | 30 |

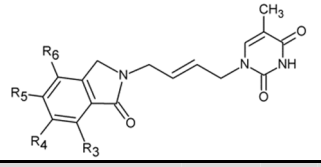


| Inhibitor | Structure | | | | $\Delta\Delta H_{MM}$ | $\Delta\Delta G_{sol}$ | $\Delta\Delta TS$ | $\Delta\Delta G_{com}$ | $K_i^{pre}$ [nM] |
|---|---|---|---|---|---|---|---|---|---|
| | $R_3$ | $R_4$ | $R_5$ | $R_6$ | | | | | |
| THMA20 | H | H | H | H | -29.06 | 1.70 | 0.52 | -27.88 | 1.31 |
| THMA21 | H | H | $NO_2$ | H | -21.02 | -1.97 | 0.96 | -23.95 | 4.7 |
| THMA22 | H | H | $NH_2$ | H | -19.45 | -1.95 | 0.68 | -22.08 | 8.7 |
| THMA23 | H | H | COO(-) | H | -27.06 | 2.11 | 0.95 | -25.9 | 2.5 |
| THMA24 | H | COO(-) | H | H | -27.15 | 8.12 | 0.91 | -19.94 | 18 |
| THMA25 | H | H | $NHCOCH_3$ | H | -26.08 | 1.61 | 1.09 | -25.55 | 2.80 |
| THMA26 | $CH_3$ | H | $NHCOCH_3$ | H | -27.45 | -1.83 | 0.99 | -30.28 | 0.60 |
| THMA27 | $CH_2CH_3$ | H | $NHCOCH_3$ | H | -39.69 | 6.97 | 1.27 | -33.99 | 0.18 |
| THMA28 | H | H | $OCH_3$ | H | -23.28 | 7.09 | 0.50 | -16.7 | 51 |
| THMA29 | H | $OCH_3$ | $OCH_3$ | H | -24.82 | 1.11 | 1.05 | -24.75 | 4 |
| THMA30 | $CH_3$ | $OCH_3$ | $OCH_3$ | H | -23.00 | 0.86 | 1.13 | -23.27 | 6 |
| THMA31 | Cl | Cl | Cl | Cl | -20.18 | -7.84 | 0.86 | -28.88 | 0.94 |

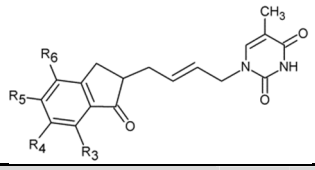


| Inhibitor | Structure | | | | $\Delta\Delta H_{MM}$ | $\Delta\Delta G_{sol}$ | $\Delta\Delta TS$ | $\Delta\Delta G_{com}$ | $K_i^{pre}$ [nM] |
|---|---|---|---|---|---|---|---|---|---|
| | $R_3$ | $R_4$ | $R_5$ | $R_6$ | | | | | |
| THMA32 | H | H | H | H | -18.84 | 5.18 | 0.57 | -14.23 | 114 |
| THMA33 | H | H | $NH_2$ | H | -20.54 | -2.13 | 0.96 | -23.63 | 5 |
| THMA34 | H | H | $OCH_3$ | H | -24.37 | -9.06 | 1.17 | -34.6 | 0.15 |
| THMA35 | H | $OCH_3$ | $OCH_3$ | H | -22.61 | 0.04 | 1.04 | -23.61 | 5 |
| THMA36 | $NH_2$ | H | $OCH_3$ | H | -19.31 | -2.91 | 0.93 | -23.15 | 6 |
| THMA37 | COO(-) | H | $OCH_3$ | H | -13.22 | -7.17 | 1.12 | -14.48 | 105 |
| THMA38 | H | H | NHCOOH | H | -25.28 | 0.56 | 1.09 | -25.81 | 2.6 |
| THMA39 | H | H | $OCH_2CO_2^-$ | H | -32.82 | 19.95 | 1.29 | -14.16 | 117 |
| THMA40 | H | H | $COOC_2H_5$ | H | -26.75 | 2.86 | 1.22 | -25.11 | 3 |
| THMA41 | $CH_2CO_2^-$ | H | $OCH_3$ | H | -19.89 | 9.74 | 1.25 | -11.41 | 287 |
| THMA42 | H | H | $OCH_3$ | $OCH_3$ | -26.37 | 2.16 | 0.98 | -25.19 | 3 |
| THMA43 | H | H | $NHCOCH_3$ | H | -27.99 | 1.34 | 1.08 | -27.73 | 1.37 |
| THMA44 | H | H | COO(-) | H | -32.07 | 21.52 | 0.95 | -11.5 | 278 |

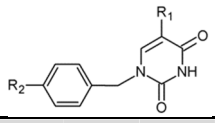


| Inhibitor | $R_1$ | $R_2$ | $\Delta\Delta H_{MM}$ | $\Delta\Delta G_{sol}$ | $\Delta\Delta TS$ | $\Delta\Delta G_{com}$ | $K_i^{pre}$ [nM] |
|---|---|---|---|---|---|---|---|
| THMA45 | Br | $CHOH(CH_2)_2CO_2^-$ | -50.51 | 30.22 | 1.07 | -21.36 | 11 |
| THMA46 | Br | $CHOH(CH_2)_2CO_2CH_3$ | -27.41 | 19.00 | 1.21 | -9.63 | 514 |
| THMA47 | Br | $(CHOH)_2CH_2CO_2^-$ | -52.01 | 34.75 | 1.19 | -18.45 | 29 |
| THMA48 | $CH_3$ | $CHOH(CH_2)_2CO_2^-$ | -50.30 | 30.22 | 0.68 | -20.76 | 13 |
| THMA49 | Br | $CHOH(CH_2)_2OCH_3$ | -46.22 | 8.83 | 0.96 | -38.35 | 0.05 |
| THMA50 | $CH_3$ | $CHOH(CH_2)_2OCH_3$ | -45.98 | 8.68 | 0.51 | -37.81 | 0.06 |

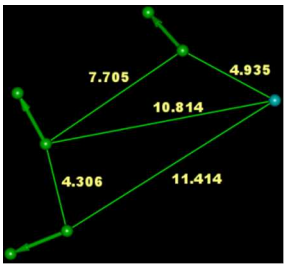


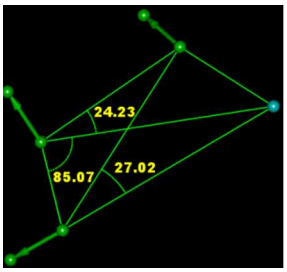


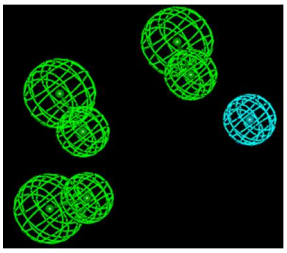

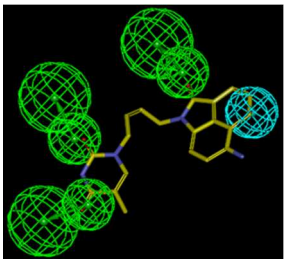

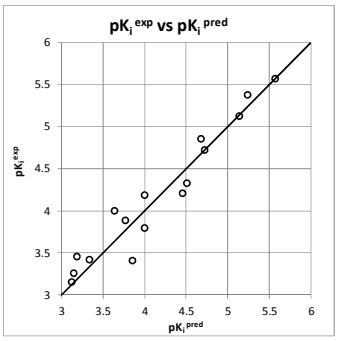


**Figure 8.** Coordinates (top), features (middle left) and mapping (middle right) of the $TMPK_{mt}$ inhibition pharmacophore with THMV3 (yellow). The correlation plot experimental vs. predicted inhibitory activity is displayed at the bottom.

## *New inhibitors*

The design of new analogs in this work is based either on the favourable features of the naphtholactam, phthalimide, isoindoline and indanone moieties linked via 2-butene spacer to the thymine or the carboxylic, hydroxymethyl moiety via aromatic spacer, Table 5, [5, 6]. We have noticed that certain substitutions in positions 4 to 7 of the naphtholactam ring and in positions of 3 to 6 of the related phthalimide, isoindoline and indanone moieties with a reduced size lead to elevated predicted binding affinities of the modelled analogs to the $TMPK_{mt}$ due to favourable attractive interactions of the substituents with the cationic residues Lys13 and Arg14, which are located in the vicinity of the substitution sites. This is the reason why some of the novel analogs (THMA1-50, Table 5) bearing negatively charged substituent in some of these positions were predicted to display inhibition potencies in the picomolar range. The $K_i^{pre}$ were calculated from the regression equation of the QSAR model of $TMPK_{mt}$ inhibition by THMDs (Table 3). The substitutions and molecular scaffolds considered are listed for the five considered categories of the THMAs in Table 5 and are shown on Figures 9 - 11.

The picomolar $K_i^{pre}$ of some designed compounds may represent a somewhat too optimistic prediction of activity that falls outside of the concentration range of the training set inhibitors considered in the QSAR model of $TMPK_{mt}$ inhibition. However, the indication of elevated inhibitory potencies of these molecules can still be a useful hint for medicinal chemists developing more potent $TMPK_{mt}$ inhibitors to explore the proposed chemical structures.

*New analogs with an aliphatic spacer*

*Substitution in positions $R_4$ to $R_7$ of the naphtholactam moiety*

These analogs THMA1-11 are derived from the most potent training set inhibitor THMD7 (Figure 4) and are intended to involve Lys13 and Arg14 residues into inhibitor binding. The best of them THMA6, which bears two hydroxymethyl groups in the positions $R_5$ and $R_6$ reached predicted inhibitory potency towards the $TMPK_{mt}$ $K_i^{pre}$ = 4 nM (Figure 9).

*Replacement of the naphtholactam by phthalimide moiety*

Replacement of the bulky naphtholactam moiety by a smaller less hydrophobic phthalimide was not favourable for the analogue binding. Substitution with a methoxy group at position 4 in THMA17 resulted in a predicted $K_i^{pre}$ of 4 nM. Surprisingly placement of a carboxyl group to the $R_4$ position in THMA16 did not lead to the expected favourable interaction with Arg14. Despite the fact that the HB between the negatively charged carboxyl oxygen and Arg14 is conserved the potency remained almost unchanged ($K_i^{pre}$ = 6 nM) with respect to THMA17, due in part to the $COO^{(-)}$ group's repulsive interaction with Glu124 and Glu166 in THMA16.

*Removal of one ketone from phthalimido moiety*

When the phthalimido moiety was replaced by an isoindoline the predicted activity increased almost 30 times c.f. THMA12 ($K_i^{pre}$ = 33 nM) and THMA20 ($K_i^{pre}$ = 1.31 nM), most probably due to unfavourable interaction of the ketone oxygen with the hydroxyl group of Tyr39 (Figure 9). Additional substitutions at positions 3 and 5 by methyl and methylamide groups, respectively (THMA26) or alternatively by chlorines in positions $R_1$ to $R_4$ (THMA31) resulted in predicted subnanomolar inhibitory potencies of the designed analogs c.f. THMA27.

*Removal of nitrogen atom from 5 membered isoindoline ring*

When the isoindoline is replaced by an 1-indanone by replacement of the $sp^2$ ring nitrogen with a $sp^3$ methylene group the predicted activity of the analogs drops by two orders of magnitude, c.f. THMA20 ($K_i^{pre}$ = 1.31 nM) and THMA32 ($K_i^{pre}$ = 114 nM). However, this substitution confers higher flexibility and improved spatial orientation of the indanone moiety. Substitutions in position $R_5$ by methoxy or acetamide groups led to analogs with predicted low nanomolar and subnanomolar inhibitory potencies (THMA34 and THMA43). The attachment of anionic carboxyl $–COO^{(-)}$ and especially methoxyacetate $–OCH_2COO^{(-)}$ groups into the $R_5$ position added two hydrogen bonds of the THMA39 to the residues Arg14 and Arg74 (Figure 9), but resulted in a relatively weak predicted binding affinity due to unfavorable solvent effect and anionic inhibitor desolvation.

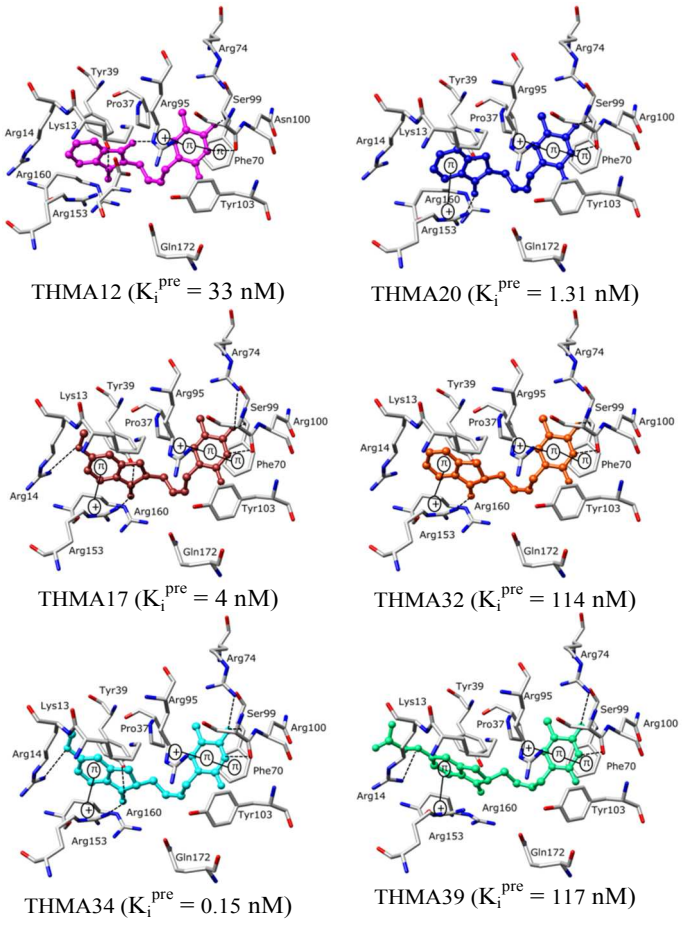


THMA12 ($K_i^{pre}$ = 33 nM) THMA20 ($K_i^{pre}$ = 1.31 nM)

THMA17 ($K_i^{pre}$ = 4 nM) THMA32 ($K_i^{pre}$ = 114 nM)

THMA34 ($K_i^{pre}$ = 0.15 nM) THMA39 ($K_i^{pre}$ = 117 nM)

**Figure 9**. Some of the most active designed analogs are shown at the active site of $TMPK_{mt}$ in stick representation. Hydrogen bonds are

shown in black dashed lines, other important interactions are shown as solid black lines.

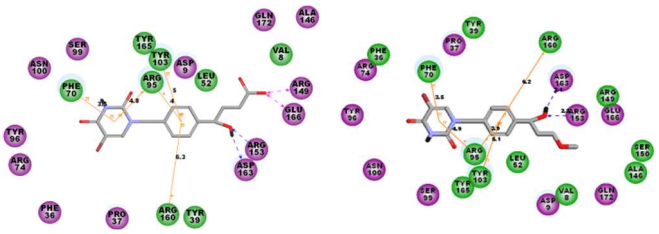

THMA45 ($K_i^{pre}$ = 11 nM) THMA49 ($K_i^{pre}$ = 0.05 nM)

**Figure 10**. 2D depiction of interaction between $TMPK_{mt}$ and THMA45 with aromatic spacer at the enzyme's active site, cation-aromatic π and aromatic π - π interactions are in orange line, HBs are in dashed blue line and charge interactions in dashed purple line.

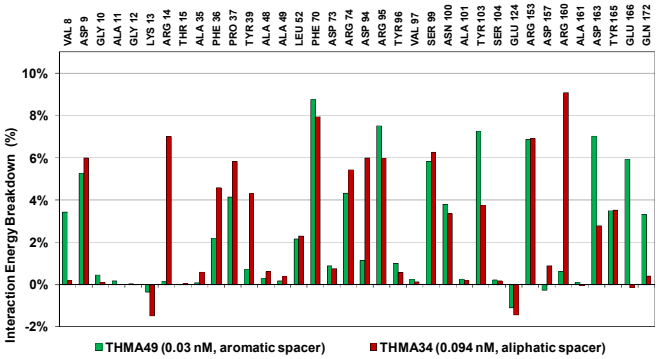


**Figure 11**. Interaction energy breakdown to residue contributions for the best designed analogs with aliphatic spacer (THMA34, red) and with aromatic spacer (THMA49, green).

**Table 6.** Predicted ADME-related Properties of some THMDs and known antituberculotics either in use or in test computed by QikProp [30]

| Compounds [a] | #stars [b] | $M_w$ [c] [g.mol$^{-1}$] | $S_{mol}$ [d] [Å$^2$] | $S_{mol,hfo}$ [e] [Å$^2$] | $V_{mol}$ [f] [Å$^3$] | *RotB* [g] | $HB_{don}$ [h] | $HB_{acc}$ [i] | $logP_{o/w}$ [j] | $logS_{wat}$ [k] | $logK_{HSA}$ [l] | *logB/B* [m] | $BIP_{caco}$ [n] [nm.s$^{-1}$] | *#meta* [o] | $K_i^{exp}$ [p] [μM] | *HOA* [q] | *%HOA* [r] |
|---|---|---|---|---|---|---|---|---|---|---|---|---|---|---|---|---|---|
| THMD6 | 1 | 392.4 | 622.1 | 176.5 | 1125.1 | 5 | 1 | 7.5 | 1.8 | -4.1 | 0 | -2.0 | 47.5 | 4 | 0.75 | 3 | 67 |
| THMD7 | 0 | 383.4 | 577.7 | 162.8 | 1071.7 | 4 | 1 | 8 | 1.7 | -3.3 | -0.2 | -1.2 | 201.8 | 3 | 0.27 | 3 | 78 |
| THMD9 | 0 | 288.3 | 535.5 | 185.4 | 920.9 | 5 | 2 | 5.5 | 1.8 | -3.3 | -0.3 | -1.7 | 20.3 | 4 | 55 | 2 | 61 |
| THMD11 | 0 | 301.3 | 573.1 | 215.8 | 988.8 | 6 | 3 | 6 | 0.7 | -2.1 | -0.5 | -1.9 | 32.5 | 5 | 112 | 2 | 58 |
| THMD13 | 0 | 367.2 | 562.5 | 136.7 | 970.8 | 6 | 2 | 5.5 | 2.5 | -3.9 | -0.2 | -1.6 | 24.2 | 3 | 10 | 2 | 66 |
| THMD15 | 0 | 288.3 | 535.1 | 133.9 | 921.4 | 6 | 2 | 5.5 | 1.8 | -3.2 | -0.3 | -1.9 | 16.1 | 3 | 202 | 2 | 59 |
| *Rifampin* | 1 | 137.1 | 313.3 | 0.0 | 479.2* | 2 | 3 | 4.5 | -0.7 | 0 | -0.8 | -0.8 | 267.5 | 2 | - | 2 | 67 |
| *Isoniazid* | 4 | 123.1* | 299.3 | 0.0 | 442.6* | 1 | 2 | 5 | -0.6 | -0.5 | -0.8 | -0.7 | 298.4 | 4 | - | 2 | 67 |
| *Ethambutol* | 2 | 204.3 | 475.7 | 395.8 | 805.7 | 11 | 4 | 6.4 | -0.2 | 0.6 | -0.8 | 0.0 | 107.8 | 4 | - | 2 | 62 |
| *Pyrazinamide* | 10 | 823.0* | 1090* | 850.0* | 2300* | 25* | 6 | 20.35* | 3.0 | -3.1 | -0.3 | -2.7 | 38.2 | 11* | - | 1 | 34 |
| ***Gatifloxacin*** | 0 | 375.4 | 597.5 | 355.7 | 1093.0 | 2 | 1 | 6.8 | 0.5 | -4.0 | 0 | -0.6 | 17.0 | 1 | - | 2 | 52 |
| ***Moxifloxacin*** | 0 | 401.4 | 641.2 | 395.6 | 1167.1 | 2 | 1 | 6.8 | 1.0 | -4.7 | 0.2 | -0.6 | 20.9 | 1 | - | 2 | 56 |
| ***Rifapentine*** | 10 | 877.0* | 1024.3* | 844.9* | 2332.6* | 24* | 6 | 20.9* | 3.6 | -2.2 | -0.2 | -1.5 | 224.0 | 13* | - | 1 | 51 |
| ***Bedaquiline*** | 4 | 555.5 | 786.5 | 213.7 | 1531.7 | 9 | 1 | 3.8 | 7.6* | -6.9 | 1.7 | 0.4 | 1562.2 | 5 | - | 1 | 100 |
| ***Delamanid*** | 2 | 534.5 | 795.6 | 284.4 | 1469.9 | 7 | 0 | 6.0 | 5.8 | -7.6 | 1.0 | -1.0 | 590.9 | 2 | - | 1 | 85 |
| ***Linezolid*** | 0 | 337.4 | 554.6 | 337.2 | 995.4 | 2 | 1 | 8.7 | 0.6 | -2.0 | -0.7 | -0.5 | 507.0 | 2 | - | 3 | 79 |
| ***Sutezolid*** | 1 | 353.4 | 594.0 | 330.6 | 1046.2 | 2 | 1 | 7.5 | 1.3 | -3.4 | -0.4 | -0.4 | 449.3 | 0 | - | 3 | 82 |
| ***Ofloxacin*** | 1 | 361.4 | 580.5 | 337.0 | 1044.0 | 1 | 0 | 7.3 | -0.4 | -2.8 | -0.5 | -0.4 | 25.9 | 1 | - | 2 | 50 |
| ***Amikacin*** | 14 | 585.6 | 738.3 | 350.3 | 1499.5 | 22* | 17* | 26.9* | -7.9* | -0.2 | -2.1 | -3.5 | 0 | 14* | - | 1 | 0 |
| ***Kanamycin*** | 10 | 484.5 | 655.8 | 258.9 | 1290.9 | 17* | 15* | 22.7* | -6.7* | 2.0 | -1.4 | -3.1 | 0 | 12* | - | 1 | 0 |
| ***Imipenem*** | 0 | 299.3 | 486.5 | 259.1 | 879.4 | 8 | 3 | 7.2 | 1.0 | -1.8 | -0.7 | -1.4 | 35.0 | 3 | - | 3 | 61 |
| ***Amoxicillin*** | 2 | 365.4 | 560.8 | 164.6 | 1032.9 | 6 | 4.25 | 8.0 | -2.5 | -0.8 | -1.1 | -1.5 | 1.0 | 5 | - | 1 | 12 |
| ***Clavulanate*** | 0 | 199.2 | 396.1 | 184.6 | 629.5 | 4 | 2 | 6.5 | -0.8 | 0.3 | -1.3 | -1.3 | 13.3 | 2 | - | 2 | 42 |

[a] known compounds inhibitors with experimentally determined inhibition constants, see Table 1;
[b] drug likeness, number of property descriptors (from 24 out of the full list of 49 descriptors of QikProp, ver. 3.7, release 14) that fall outside the range of values for 95% of known drugs (range or recommended values: 0 – 5);
[c] molecular weight in g.mol$^{-1}$ (range for 95% of drugs: 130 – 725 g.mol$^{-1}$) [30];
[d] total solvent-accessible molecular surface, in Å$^2$ (probe radius 1.4 Å) (range for 95% of drugs: 300 – 1000 Å$^2$);
[e] hydrophobic portion of the solvent-accessible molecular surface, in Å$^2$ (probe radius 1.4 Å) (range for 95% of drugs: 0 – 750 Å$^2$);
[f] total volume of molecule enclosed by solvent-accessible molecular surface, in Å$^3$ (probe radius 1.4 Å) (range for 95% of drugs: 500 – 2000 Å$^3$);
[g] Number of non-trivial (not CX3), non-hindered (not alkene, amide, small ring) rotatable bonds (range for 95% of drugs: 0 – 15);
[h] Estimated number of hydrogen bonds that would be donated by the solute to water molecules in an aqueous solution. Values are averages taken over a number of configurations, so they can be non-integer (range for 95% of drugs: 0.0 – 6.0);
[i] Estimated number of hydrogen bonds that would be accepted by the solute from water molecules in an aqueous solution. Values are averages taken over a number of configurations, so they can be non-integer (range for 95% of drugs: 2.0 – 20.0);
[j] logarithm of partitioning coefficient between n-octanol and water phases (range for 95% of drugs: -2 – 6.5);
[k] logarithm of predicted aqueous solubility, log S. S in mol dm$^{-3}$ is the concentration of the solute in a saturated solution that is in equilibrium with the crystalline solid (range for 95% of drugs: -6.0 – 0.5);
[l] logarithm of predicted binding constant to human serum albumin (range for 95% of drugs: -1.5 – 1.5);
[m] logarithm of predicted brain/blood partition coefficient. Note: QikProp predictions are for orally delivered drugs so, for example, dopamine and serotonin are CNS negative because they are too polar to cross the blood-brain barrier (range for 95% of drugs: -3.0 – 1.2);
[n] predicted apparent Caco-2 cell membrane permeability in Boehringer-Ingelheim scale, in [nm/s] (range for 95% of drugs: < 25 poor, > 500 great);
[o] number of likely metabolic reactions (range for 95% of drugs: 1 – 8);
[p] experimental *THMD* inhibitory activity [6,12,13];
[q] human oral absorption (1-Low, 2-Medium, 3-High);
[r] percentage of human oral absorption in gastrointestinal tract (<25% - poor, >80% high);
(*) star indicating that the property descriptor value falls outside the range of values for 95% of known drugs.

*New analogs with aromatic spacer*

The training set THMDs is composed with almost 50% aliphatic spacer (*al*THMDs, $0.27 \leq K_i^{exp} \leq 6$ μM) and 50% aromatic spacer (*ar*THMDs, $10 \leq K_i^{exp} \leq 202$ μM). At first sight and according to their potency it seems obvious that designed *ar*THMAs will never reach the potency level of *al*THMAs. The analysis of residues contribution to $E_{int}$ breakdown for THMD13 (the best *ar*THMDs in the training set) in Figure 6 shows that the three additional interactions between the aromatic spacer ring and residues Arg95 and Arg160 (cation - π) and Tyr103 (π - π) raise substantially the affinity towards $TMPK_{mt}$. Moreover as depicted in 2D in Figure 10 and the graph in Figure 11 the carboxylic group repulsive interactions with Glu124 and Glu166 lowers the affinity (THMA45, 47 and 48). Oppositely the methoxy group enhances the THMAs stabilizing interactions with the enzyme exemplified by THMA49 and 50. Besides the basic stacking involving the thymine moiety common to both *al*THMAs and *ar*THMAs, these three additional π - π and cation - π interactions and finally two HBs between the OH on $R_2$ and Arg153 and Asp163 justify the significant increase of the predictive potency exhibited by *ar*THMAs.

The overall contribution to $E_{int}$ of the residues specific for $TMPK_{mt}$ of 15% for THMA34 vs. 5% for THMA49 breakdown into residue contributions: Arg14 (7% – THMA34 vs. 0% – THMA49), Tyr39 (4% – THMA34 vs. 1% – THMA49) and Asn100 (4% – THMA34 vs. 4% – THMA49) render the best *ar*THMA less selective than its *al*THMA counterpart. For *ar*THMAs the conversion of the carboxylic acid group (THMA45, $K_i^{pre}$ = 8 nM) into a bulkier methyl ester resulted in a detrimental decrease of affinity (THMA46, $K_i^{pre}$ = 458 nM).

## *ADME-related Properties of THMA Inhibitors*

Drug likeness parameter (#stars, for definition see the Methods section) computed for known THMD inhibitors of $TMPK_{mt}$, antituberculotics either in clinical use or in clinical trials (Table 6) and selected potent designed analogs THMAx (Table 7) characterizes the ADME related properties relevant for the pharmacokinetic profile of a compound. As we can see from Tables 6 and 7, the most potent THMDs as well as the predicted most active designed THMAs display favourable values of #stars parameter equal to 0 for all except one compound. Five of the novel antituberculosis drugs in trials also display #stars equal to zero. Therefore, the designed THMA analogs are predicted to possess favourable pharmacokinetic profiles and thus represent suitable candidates for synthesis and experimental testing.

The most active designed *al*THMAs (THMA6 and 34) and *ar*THMAs (THMA49 and 50) display pharmacokinetic profiles for almost all descriptors considered (Table 7). [30]. There is, however, a noticeable difference in the cell wall permeability parameter $BIP_{caco-2}$ (Table 7) showing that *ar*THMAs display higher predicted permeability rates than the two *al*THMAs. It is worthwhile mentioning that about 50% of new antituberculotics in (pre)clinical trials fall into low $BIP_{caco-2}$ permeability range. *ar*THMAs' predicted percentage of human oral absorption in gastrointestinal tract (HOA) falls into the range of 85% against 66% for *al*THMAs, which suggest the possibility of higher oral bioavailability for the most active *ar*THMAs [30]. According to these descriptors the *ar*THMAs analogs display more favorable predicted ADME-related profiles and drug-like properties and thus represent candidate molecules suitable for synthesis.

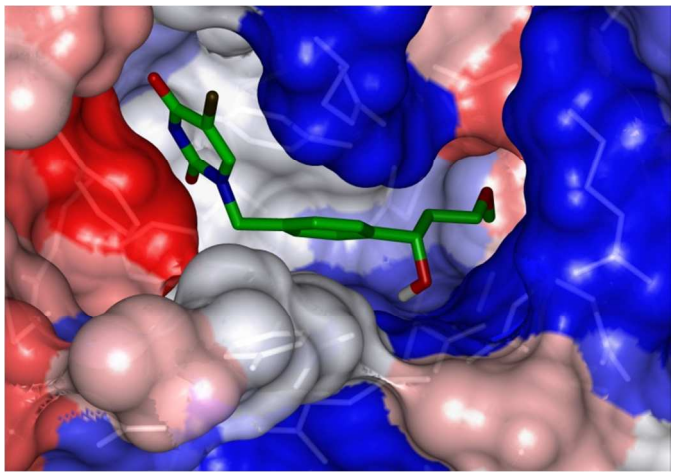

**Figure 12**. Connolly surface of the predicted most active *ar*THMA THMA49 at the active site of $TMPK_{mt}$. The binding cleft surface is coloured according to residue hydrophobicity: red-hydrophobic, blue-hydrophilic and white-intermediate residues.

## Conclusions

The high statistical significance of the QSAR model and PH4 pharmacophore model derived from a training set of 20 and validation set of 3 THMD compounds was well documented. Presence of the naphtholactam moiety in the most potent *al*THMAs $TMPK_{mt}$ inhibitors and analysis of the active site residue contributions to $E_{int}$ directed us in our effort to optimize the structures of the known inhibitors and enhance the involvement of the residues Lys13 and Arg14 in the inhibitor binding. We have replaced in *al*THMAs the bulky and rigid naphtholactam moiety by smaller less hydrophobic and more flexible phthalimide, isoindoline and indanone moieties.

**Table 7.** Predicted ADME-related Properties of Selected Most Potent Designed THMDs Analogues Computed by QikProp [30]

| Novel Analogs [a] | #stars [b] | $M_w$ [c] [g.mol$^{-1}$] | $S_{mol}$ [d] [Å$^2$] | $S_{mol,hfo}$ [e] [Å$^2$] | $V_{mol}$ [f] [Å$^3$] | *RotB* [g] | $HB_{don}$ [h] | $HB_{acc}$ [i] | $logP_{o/w}$ [j] | $logS_{wat}$ [k] | $logK_{HSA}$ [l] | *logB/B* [m] | $BIP_{caco}$ [n] [nm.s$^{-1}$] | *#meta* [o] | $K_i^{pred}$ [p] [nM] | *HOA* [q] | *%HOA* [r] |
|---|---|---|---|---|---|---|---|---|---|---|---|---|---|---|---|---|---|
| THMA6 | 0 | 407.4 | 634.3 | 245.4 | 1174.3 | 8 | 3 | 9.9 | 1.1 | -3.2 | -0.3 | -2.0 | 70.6 | 5 | 3 | 3 | 66 |
| THMA12 | 0 | 325.3 | 546.4 | 170.1 | 971.3 | 4 | 1 | 6.5 | 1.7 | -3.4 | -0.1 | -1.2 | 207.2 | 3 | 21 | 3 | 79 |
| THMA28 | 0 | 341.4 | 590.1 | 290.9 | 1058.0 | 5 | 1 | 7.3 | 2.0 | -3.6 | -0.1 | -1.2 | 341.5 | 5 | 33 | 3 | 84 |
| THMA32 | 0 | 310.4 | 571.3 | 216.4 | 1002.9 | 4 | 1 | 5.5 | 2.5 | -4.1 | 0.1 | -1.1 | 379.2 | 5 | 77 | 3 | 88 |
| THMA34 | 0 | 384.4 | 639.2 | 309.7 | 1147.6 | 6 | 2 | 8.3 | 2.0 | -4.1 | -0.3 | -2.0 | 17.2 | 6 | 0.094 | 2 | 61 |
| THMA39 | 0 | 384.4 | 669.8 | 262.1 | 1174.7 | 7 | 2 | 8.3 | 1.9 | -4.4 | -0.3 | -2.6 | 7.1 | 7 | 101 | 2 | 54 |
| THMA49 | 0 | 369.2 | 557.8 | 200.4 | 976.7 | 7 | 2 | 6.9 | 1.9 | -3.3 | -0.3 | -1.0 | 396.6 | 3 | 0.03 | 3 | 85 |
| THMA50 | 0 | 304.3 | 560.9 | 286.1 | 983.8 | 7 | 2 | 6.9 | 1.7 | -3.0 | -0.3 | -1.2 | 426.5 | 4 | 0.04 | 3 | 84 |

[a] see Table 5 for the chemical structures of the virtual hits;
[b] to [r] except p see the footnote of Table 6;
[p] predicted $K_i^{pre}$ s were estimated from the QSAR equation, Table 3;

Additional substitutions with methoxy, hydroxy-methyl and acetamide groups in positions $R_4$ and $R_5$ of the aromatic scaffolds improved the binding site interactions by specific hydrogen bonding involving the Lys13, Arg14, Arg153 and Tyr39 residues to reach 0.15 nM predicted potency. These residues were identified and targeted based on the active site interaction energy $E_{int}$ breakdown for a molecular mechanics all-atom model of inhibitor-$TMPK_{mt}$ binding and comparative analysis, which led to identification of new potent inhibitor candidates. In the same way replacement of the butenyl spacer of *al*THMAs by an aromatic one in *ar*THMAs intensifies the affinity by adding three $\pi$ - $\pi$ and cation - $\pi$ interactions and two HBs to reach picomolar predicted potency.

Although our activity predictions may be somewhat too optimistic, they still point to a specific subset of the chemical space which may contain subnanomolar $TMPK_{mt}$ inhibitors with favourable pharmacokinetic profiles. A more systematic search through screening of combinatorial library targeted around our designed inhibitors THMA34, THMA27, THMA48 and THMA49 and subsequent activity evaluation in an enzymatic assay may lead to a discovery of new potent antituberculotics.

## Notes and references

[a] ICS-UNIDO, Area Science Park, Padriciano 99, Trieste I-34012, Italy.
[b] Molecular and Structural Biology Division, Central Drug Research Institute, Lucknow 226001,CSIR, India. E-mail: imsiddiqi@yahoo.com
[c] Zhang Initiative Research Unit, Advanced Science Institute, RIKEN, 2-1 Hirosawa, Wako, Saitama 351-0198, Japan. E-mail: ashucdri@gmail.com
[d] University of Abobo Adjamé, UFR SFA, Laboratoire de Physique Fondamentale et Appliquée, 02 BP 801, Abidjan 02, Cote D'Ivoire. E-mail: keitamelalie@yahoo.fr, dalibrice@yahoo.fr
[e] Department of Physical Chemistry of Drugs, Faculty of Pharmacy, Comenius University, SK-83232 Bratislava, Slovakia. E-mail: frecer@fpharm.uniba.sk
[f] International Centre for Applied Research and Sustainable Technology, SK-84104 Bratislava, Slovakia.
[g] Faculty of Natural Sciences, University of Ss. Cyril and Methodius, 91701 Trnava, Slovakia. E-mail: stanislav.miertus@icarst.org
[*] *Corresponding author:* Eugène Megnassan, University of Abobo Adjamé, UFR SFA, Laboratoire de Physique Fondamentale et Appliquée, 02 BP 801, Abidjan 02, Cote D'Ivoire, E-mail: megnase@yahoo.com

1 C. Dye, D. Maher, D. Weil, et al., *Int. J. tuberculosis Lung Dis.,* 2006, **10,** 460-462.
2 A. Zumla, M. Raviglione and R. Hafner, F. von Reyn, *New Engl. J. Med.,* 2013, **368**, 745-755.
3 Global tuberculosis report 2012. Geneva: World Health Organization (http:// www.who.int/tb/publications/global_report/en/).
4 A. Haouz, V. Vanheusden, H. Munier-Lehmann, et al., *J. Biol. Chem.,* 2003, **278,** 4963-4971.
5 V. Vanheusden, P.V. Rompaey, H. Munier-Lehmann, et al., *Bioorg. Med. Chem. Lett.,* 2003, **13**, 3045-3048.
6 O. Familiar, H. Munier-Lehmann, A. Negri, et al., *ChemMedChem*, 2008, **3**, 1083-1093.
7 B. Gopalakrishnan, V. Aparna, J. Jeevan, et al., *J. Chem. Inf. Model.,* 2005,**45,** 1101-1108.
8 T. Ursby, M. Weik, E. Fioravanti, et al., *Acta Crystallogr.,* 2002, *D***58,** 607-614.
9 I. Li de la Sierra, H. Munier-Lehmann, A.M. Gilles, et al., *J. Mol. Biol.,* 2001, **311**, 87-100.
10 V. Frecer, P. Seneci, S. Miertus, *J. Comput.-Aided Mol. Des.,* 2011, **25**, 31-49.
11 L.C. Owono Owono, M. Keita, E. Megnassan, et al., *Tuberculosis Res. Treat.,* 2013, **2013**, 1-13, ID 670836.
12 S. Pochet, L. Dugue, G. Labesse, et al., *ChemBioChem,* 2003, **4,** 742-747.
13 C. Gasse, D. Douguet, V. Huteau, et al., *Bioorg. Med. Chem.*, 2008, **16**, 6075-6085.
14 H.M. Berman, J. Westbrook, G.Z. Feng, et al., *Nucl. Acids Res.*, 2000, **28**, 235-242.
15 Discovery Studio molecular modeling and simulation program, version 2.5, Accelrys, Inc., San Diego, CA, 2009.
16 V. Frecer, S. Miertus, A. Tossi, D. Romeo, *Drug Des. Discov.,* 1998, **15**, 211-231.
17 V. Frecer, S. Miertus, *Macromol. Chem. Phys.,* 2002, **203**, 1650-1657.
18 V. Frecer, F. Berti, F. Benedetti, S. Miertus, *J. Mol. Graphics Modell.*, 2008, **27**, 376-387.
19 B. Dali, M. Keita, E. Megnassan, et al., *Chem. Biol. Drug Des.,* 2012, **79**, 411-430.
20 E. Megnassan, M. Keita, C. Bieri, et al., *Med. Chem.,* 2012, **8**, 5, 970-984.
21 M.K. Gilson, B. Honig, *J. Comp.-Aided Mol. Des*., 1991, **5**, 5-20.
22 W. Rocchia, S. Sridharan, A. Nicholls, et al., *J. Comput. Chem.*, 2002, **23**, 128-137.
23 Böttcher C.J.F, "Theory of Electric Polarization", *Elsevier Press,* Amsterdam, 1973.

24 S. Miertus, E. Scrocco, J. Tomasi, *Chem. Phys.*, 1981, **55**, 117-129.
25 V. Frecer, S.Miertus, *Int. J. Quant. Chem.*, 1992, **42**, 1449-1468.
26 S. Fischer, J.C. Smith, C. Verma, *J. Phys. Chem. B*, 2001, **105**, 8050-8055.
27 S.M. Schwarzl, T.B. Tschopp, J.C. Smith, S. Fischer, *J. Comput. Chem.*, 2002, **23**, 1143-1149.
28 Tirado-Rives, J.; Jorgensen W. L., *J. Med. Chem.* 2006, 49, 5880-5884
29 H. Li, J. Sutter, R. Hoffmann, "In: *Pharmacophore Perception, Development and Use in Drug Design*", *O.F. Güner, Ed.*, International University Line: La Jolla, CA, USA, 2000, 171-189.
30 QikProp, version 3.7, release 14, X Schrödinger, LLC, New York, NY, 2014.
31 Duffy E.M.; Jorgensen W.L., *J. Am. Chem. Soc.* 2000, 122, 2878-2888.
32 Jorgensen W.L., Duffy E.M., *Bioorg. Med. Chem. Lett.* 2000, 10, 1155-1158.
33 Jorgensen W.L., Duffy E.M., *Adv. Drug Delivery Rev.* 2002, 54, 355-366.